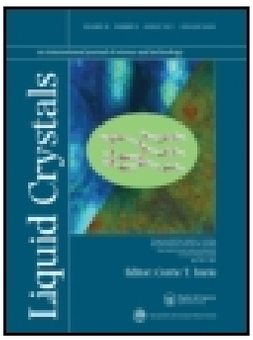

Liquid Crystals

ISSN: 0267-8292 (Print) 1366-5855 (Online) Journal homepage: http://www.tandfonline.com/loi/tlct20

High performance LCD for augmented reality and virtual reality displays

Javed Rouf Talukder, Yuge Huang & Shin-Tson Wu

To cite this article: Javed Rouf Talukder, Yuge Huang & Shin-Tson Wu (2018): High performance LCD for augmented reality and virtual reality displays, Liquid Crystals, DOI: 10.1080/02678292.2018.1540067

To link to this article: https://doi.org/10.1080/02678292.2018.1540067

Published online: 30 Oct 2018.

LIQUID CRYSTALS
https://doi.org/10.1080/02678292.2018.1540067

Taylor & Francis
Taylor & Francis Group

High performance LCD for augmented reality and virtual reality displays

Javed Rouf Talukder, Yuge Huang and Shin-Tson Wu

College of Optics and Photonics, University of Central Florida, Orlando, FL, USA

ABSTRACT

For augmented reality and virtual reality displays, high-resolution density, high luminance, and fast response time are critically needed. High-resolution density helps eliminate the screen-door effect; high luminance and fast response time enable low duty ratio operation, which plays a key role for suppressing image blurs. By using a low viscosity material and new diamond-shaped electrode configuration, we demonstrate a fringe field switching liquid crystal display, abbreviated as d-FFS LCD, with high transmittance, fast grey-to-grey response time, low operation voltage, wide viewing angle, and indistinguishable colour shift and gamma shift. We also investigate the rubbing angle (α) effects on transmittance and response time. When α = 0°, the virtual wall effect is strong, resulting in fast response time but compromised transmittance. When α ≥ 1.2°, the virtual walls disappear, as a result, the transmittance increases dramatically, but the trade-off is in slower response time.

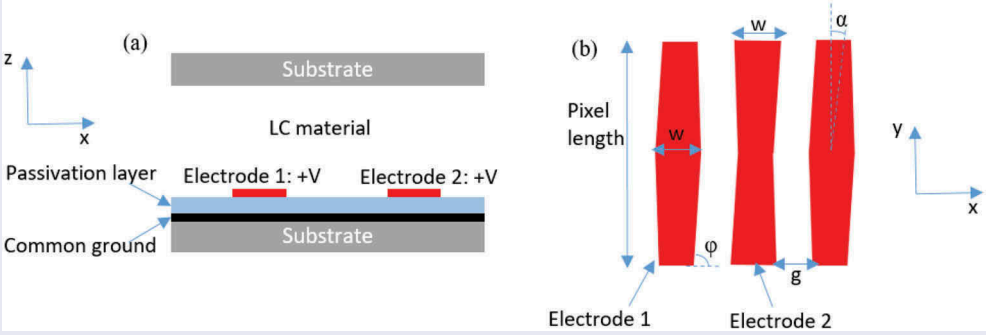

ARTICLE HISTORY
Received 30 September 2018
Accepted 21 October 2018

KEYWORDS
Liquid crystals; augmented reality; virtual reality; displays

1. Introduction

Presently, thin-film-transistor (TFT) liquid crystal display (LCD) and organic light-emitting diode (OLED) displays are two dominating technologies for TVs, smartphones, and augmented reality (AR) and virtual reality (VR) [1–4]. Although each technology has its own pros and cons [5], a common demand is higher resolution density and fast response time. This is particularly important for AR and VR displays in order to mitigate the annoying screen door effect. However, as the resolution density increases, the display luminance decreases because of the reduced aperture ratio. Lower optical efficiency leads to increased power consumption, i.e. shorter battery lifetime for mobile displays. Another equally important performance metric is image blur, which is governed by the motion picture response time (MPRT) [6]. MPRT is jointly determined by the TFT frame rate, LCD/OLED response time and duty ratio [7]. Both active matrix LCD and OLED are holding type displays; thus, they would exhibit different degree of image blurs. Under the same frame rate, say 120 Hz, if an LCD's response time is below 2 ms, then its MPRT is comparable to that of OLED, even its response time is as fast as 1 μs. A common approach to suppress the image blur of LCD and OLED is to lower the duty ratio [7] so that they behave CRT-like impulse driving. However, to keep the same luminance, say 150 nits for VR, we have to boost LCD's backlight brightness or OLED's driving current. As a result, efficiency droop in LED backlight [8] takes place or OLED's lifetime is compromised [9]. Therefore, a high transmittance and fast MPRT LCD is urgently needed for the emerging AR and VR displays.

Fringe field switching (FFS) LCD [10] is a favourable choice for high-resolution density panels because of its built-in storage capacitor and weak colour shift. The former enables high-resolution density. However, FFS still has some room for improvement, such as limited contrast ratio (CR ~2000:1) and relatively slow response time (10–15 ms due to the small twisted elastic constant K_{22}

CONTACT Shin-Tson Wu swu@ucf.edu

Table 1. Measured physical properties of M1 at T = 25°C and f = 1 kHz.

LC mixture	Δn @ λ = 550 nm	$\varepsilon_{//}$	$\varepsilon_{\square}$	Δε	γ_1 (mPa· s)	K_{11} (pN)	K_{22} (pN)	T_m (°C)	T_c (°C)	E_a (meV)
M1	0.1225	5.53	2.87	2.66	35.75	9.93	6.03	−34.5	76.7	248.1

involved). To improve contrast ratio, mini-LED backlight with area local dimming has been implemented and remarkable result (CR >10^5:1) has been achieved [11,12]. To shorten response time, interdigitated pixel-electrode structures with two-dimensional standing layers (also called virtual walls) have been proposed [13–16]. These virtual walls exert an additional restoring torque to accelerate the decay process so that the average grey-to-grey (GTG) response time can be reduced to 3–5 ms. However, a significant trade-off is compromised transmittance due to the existence of virtual walls.

In this paper, we report a new FFS LCD with diamond-shaped electrode structure along with a low-viscosity LC mixture to simultaneously achieve high transmittance and fast GTG response time, while preserving the inherent advantages on wide-viewing angle and indistinguishable gamma shift and colour shift. Its application for high-resolution density displays is emphasised.

2. LC material

To obtain high transmittance in a thin cell gap (e.g. 2.5–3.0 μm), we should use a slightly higher birefringence (Δn ~0.12) LC material. Meanwhile, a modest dielectric anisotropy ($\Delta\varepsilon = \varepsilon_{//} - \varepsilon_{\square}$) is required for keeping operation voltage below 6 V. However, the polar groups contributing to enhance Δε will also lead to an increased viscosity. To achieve high transmittance and fast response time, while keeping low operation voltage, we formulated a high Δn LC mixture with balanced dielectric anisotropy and viscosity. Actually, DIC-LC2 (DIC Corp.) exhibits a very low rotational viscosity and relatively high birefringence, except that its dielectric anisotropy is somewhat too small (Δε ≈ 1.7 at 21°C) [17]. Therefore, to increase Δε, we mixed 80.9% DIC-LC2 with 19.1% DIC-LC3 (Δε ≈ 8.8). For convenience, we call this experimental mixture as M1. The measured rotational viscosity (γ_1), birefringence, dielectric anisotropy, splay elastic constant (K_{11}), twist elastic constant (K_{22}), and activation energy (E_a) are listed in Table 1. Melting temperature (T_m) and clearing temperature (T_c) were measured by Differential Scanning Calorimetry (DSC, TA instruments Q100).

2.1. Birefringence

To measure the birefringence of M1, we used a commercial homogeneous cell with cell gap 7.65 μm. After injecting M1 into a homogeneous cell, we placed the cell on a Linkam heating stage which was controlled by TMS94 temperature programmer. We then sandwiched this cell between crossed polarisers and applied 1-kHz square-wave AC voltage to this LC cell. A He-Ne laser (λ = 633 nm) was used as probing beam. Birefringence was calculated from the measured phase retardation. Figure 1(a) depicts the temperature-dependent birefringence at λ = 633 nm, where dots are measured data and solid red line is fitting with Haller's semi-empirical equation [18]:

$$\Delta n = \Delta n_0 S = \Delta n_0 (1 - T/T_c)^{\beta}. \quad (1)$$

In Equation (1), T is the Kelvin temperature, T_c is the clearing point of LC, Δn_0 is the extrapolated birefringence at T = 0, S is the order parameter and β is a material constant. From fittings, we obtained Δn_0 = 0.1681 and β = 0.1851 for M1.

Next, we measured the wavelength dispersion of M1 by using a He-Ne laser (λ = 633 nm) and a tunable

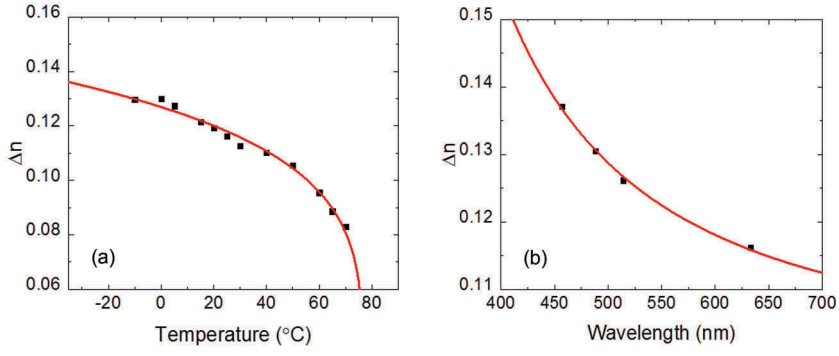

Figure 1. (a) Temperature-dependent Δn of M1 at λ = 633 nm. (b) Δn dispersion of M1 at 25°C. Dots are measured data, and the red lines in (a) and (b) are fitting curves with Equations (1) and (2), respectively.

argon ion laser (λ = 457, 488 and 514 nm). Results are plotted in Figure 1(b), where dots are measured results and solid line is the fitting curve with single-band birefringence dispersion equation [19]:

$$\Delta n = G\frac{\lambda^2\lambda^{*2}}{\lambda^2 - \lambda^{*2}}, \quad (2)$$

In Equation (2), G is the proportionality constant and λ^* is the mean resonance wavelength. Through fittings, we obtained G = 1.740 μm^{-2} and λ^* = 0.239 μm. Using these parameters and Equation (2), we find Δn = 0.138, 0.123, 0.115 at λ = 450, 550, 650 nm, respectively. Later, we will use these data in our device simulation.

2.2. Visco-elastic coefficient

To determine the visco-elastic coefficient, we measured the transient decay time of M1 in a homogeneous cell. Results are shown in Figure 2, where dots are experimental data and solid line represents the fitting with following equation [20]:

$$\frac{\gamma_1}{K_{11}} = A\frac{\exp(E_a/k_BT)}{(1 - T/T_c)^{\beta}}. \quad (3)$$

In Equation (3), A is the proportionality constant, k_B is the Boltzmann constant and E_a is the activation energy. From fittings, we obtained E_a = 248.1 meV. From Figure 2, we find γ_1/K_{11} = 3.60 ms/μm^2 at T = 25°C. Through threshold voltage measurement (not shown here), we found K_{11} = 9.93 pN, and subsequently γ_1 = 35.75 mPas at 25°C.

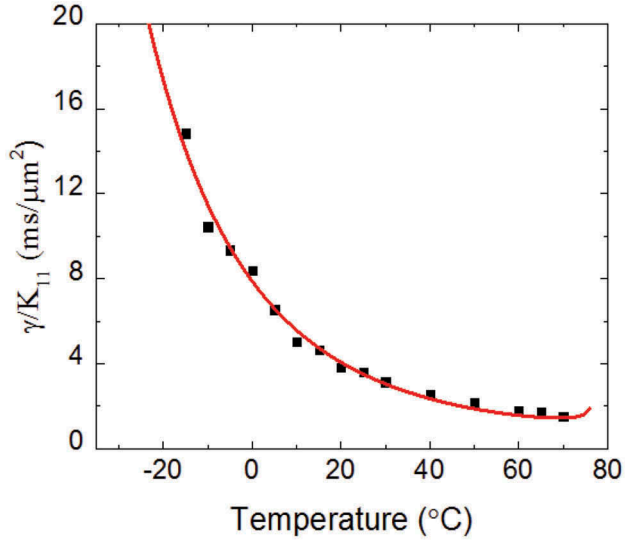

Figure 2. Temperature-dependent visco-elastic coefficient of M1 at λ = 633 nm. Dots are measured data and red line represents the fitting curve with Equation (3). The fitting parameters are listed in Table 1.

In order to obtain K_{22}, we filled M1 into a commercial IPS (in-plane switching) cell with 3-μm cell gap and measured its transient decay time [21]. From the decay time constant, we extracted γ_1/K_{22} = 5.93 ms/μm^2 at 25°C. From the already obtained γ_1, we can calculate the twist elastic coefficient and result is K_{22} = 6.03 pN. We will use these parameters in our device simulations discussed below.

3. Device structure

We propose a new device structure to achieve high transmittance using M1. Figure 3(a,b) depicts the cross-sectional and top views of our proposed electrode configuration. The top substrate has a thin surface alignment layer (not shown), while bottom substrate has a planar common electrode, a passivation layer, diamond-shaped pixel electrodes and a thin surface alignment layer (not shown). For simplicity, let us call the structure shown in Figure 3(b) as diamond-shaped FFS mode, abbreviated as d-FFS. The electrode width, electrode gap and electrode tilt angle are denoted as w, g and φ, respectively, and α is the LC alignment direction (rubbing angle) with respect to y axis.

This structure looks similar to traditional stripe structure from cross-sectional view, but it has diamond shape from top view. The reason for making it diamond shape and spatial shift between adjacent pixel electrodes is to increase the transmittance by reducing the dead zones on top of pixel electrodes [22]. The LC cell is sandwiched between two crossed linear polarisers. The LC directors are aligned along y-axis and pretilt angle is θ_p = 0. In contrast, the requirement of non-zero pretilt angle in conventional structures limits the tolerable deviation due to rubbing alignment accuracy [23]. Compared to previous report on the interdigitated pixel electrodes of FFS mode, our design significantly boosts the transmittance by reducing the dead zones on top of electrode while maintaining a comparable response time.

4. Simulation results

We simulated the LC directors distribution of d-FFS cell filled with M1 with a commercial LCD simulator Techwiz LCD 3D (Sanayi, Korea) and then calculated the electro-optic properties by using the extended 2 × 2 Jones matrix method [24]. The parameters employed in the simulation, shown in Figure 3(b), are set as follows: LC cell gap 2.5 μm, electrode width w = 2.0 μm, electrode gap g = 3.0 μm, pixel length 20 μm, pixel ITO thickness 50 nm, passivation layer thickness 150 nm, pretilt angle θ_p = 0 and electrode tilt angle φ = 88.85°. Anchoring energy of the alignment layer is assumed to be strong.

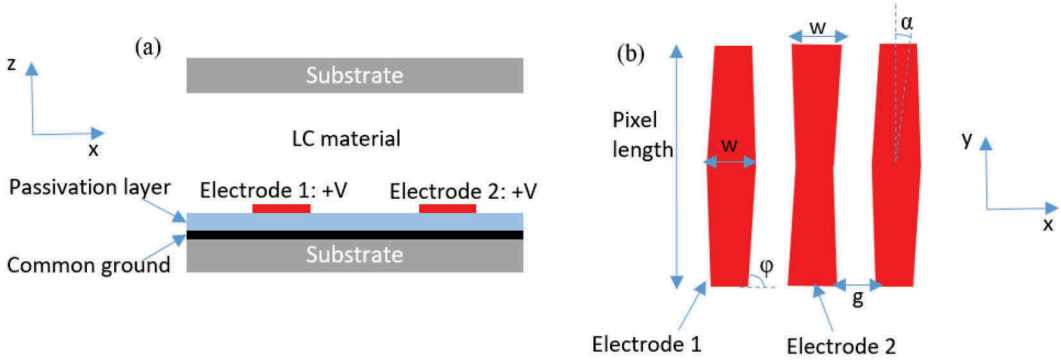

Figure 3. Schematic diagram of the proposed d-FFS structure. (a) Cross-sectional view, and (b) top view. w: electrode width, g: electrode gap, φ: electrode tilt angle and α: LC alignment direction w.r.t. *y* axis.

The LC parameters used in this calculation are listed in Table 1. The transmission axis of bottom polariser is parallel to the LC alignment direction. To explore the tolerance of LC alignment angle, we conducted simulations with two rubbing angles α = 0° and 1.5°; the former exhibits fast response time due to virtual walls, while the latter exhibits high transmittance owing to the disappearance of virtual walls, as will be explained later.

4.1. VT curves and response time

To examine at which rubbing angle the virtual walls would disappear, we calculated the response time (rise + decay) and normalised transmittance at different rubbing angles. Results are plotted in Figure 4. From Figure 4, the transmittance is the lowest and the response time is the fastest when α = 0°, due to the virtual wall effects. These standing layers exert a strong anchoring force to shorten the LC response time, but the formed dead zones reduce the transmittance significantly. As the rubbing angle increases, the virtual wall effects are gradually weakening. The onset takes place at α ≈ 1.1°; above

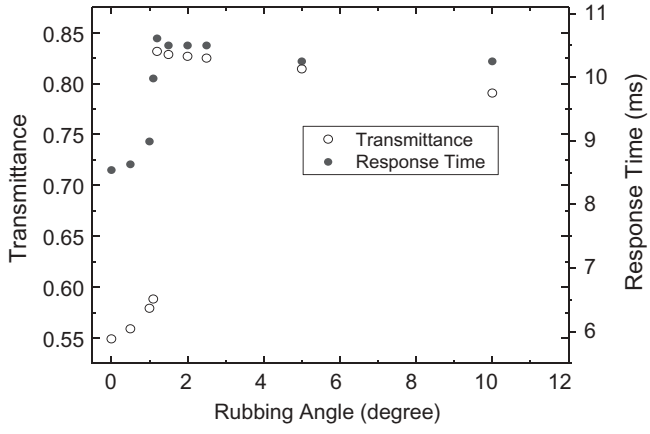

Figure 4. Simulated transmittance and response time of d-FFS at different rubbing angles.

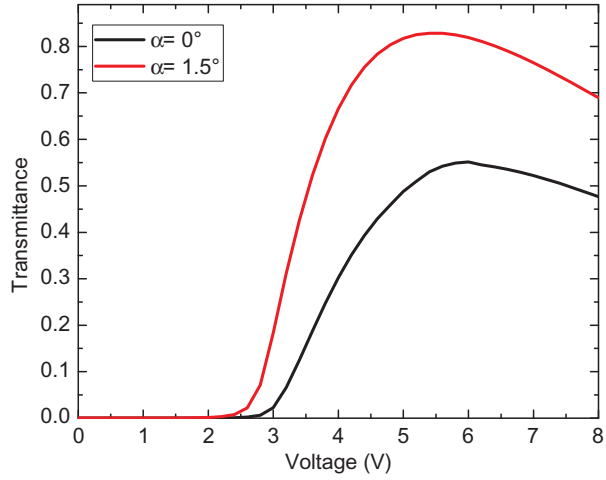

Figure 5. Simulated VT curves of d-FFS at α = 0° and 1.5°, λ = 550 nm.

α ≈ 1.2°, the transmittance increases sharply but the response time also increases. As α > 1.5°, the transmittance starts to decline gradually (due to decreased phase retardation), while response time remains more or less unchanged. Therefore, the optimal rubbing angle lies between 1.2° and 2.0°.

Figure 5 shows the simulated voltage-dependent transmittance (VT) curves at α = 0° and α = 1.5°, while keeping the LC pretilt angle at θ_p = 0. At α = 0°, the peak transmittance (at 5.8 V_{rms}) is 54.9%. Although the transmittance is relatively low, this result is comparable to those reported in [14–16]. Indeed, this is a general trade-off between response time and transmittance. However, the result at α = 1.5° is quite unexpected. Its peak transmittance reaches ~82.9% at 5.4 V_{rms}. Detailed physical mechanism will be discussed later. The increased peak transmittance is particularly desirable for high-resolution density displays, where both the aperture ratio and the optical efficiency are decreased. As will be discussed later, low backlight duty-ratio can be applied to shorten the MPRT to

1.5 ms. However, the trade-off is decreased-display luminance. Therefore, the high-transmittance d-FFS LCD offers a promising solution for suppressing image blurs while keeping a relatively high-display luminance. The latter is particularly important for the battery-powered mobile-display devices.

Low viscosity is helpful for achieving fast response time. As listed in Table 1, M1 exhibits a very low rotational viscosity (γ_1 = 35.75 mPas). Figure 6 shows the calculated time-dependent transmittance curves for d-FFS at α = 0° and 1.5°. The voltage corresponding to peak transmittance is applied to calculate the rise time and decay time. Response time is defined as the transmittance change between 10% and 90% of the maximum value.

At α = 0°, the rise time and decay time are calculated to be 5.59 and 2.95 ms, whereas at α = 1.5° the rise time and decay time are 5.75 and 4.75 ms, respectively. At α = 0°, the observed faster decay time results from the restoring force exerted by the virtual walls. In comparison, the response time of our d-FFS is faster than that of the alternating tilt device under the same rubbing angle [23] because of its slightly thinner cell gap. Our d-FFS at α = 1.5° offers ~85% transmittance (normalised to that of two parallel polarisers) and reasonably fast response time. Such a high transmittance is comparable to that of a single-domain FFS mode with a positive Δε LC, but the average GTG response time is about 2x faster [25].

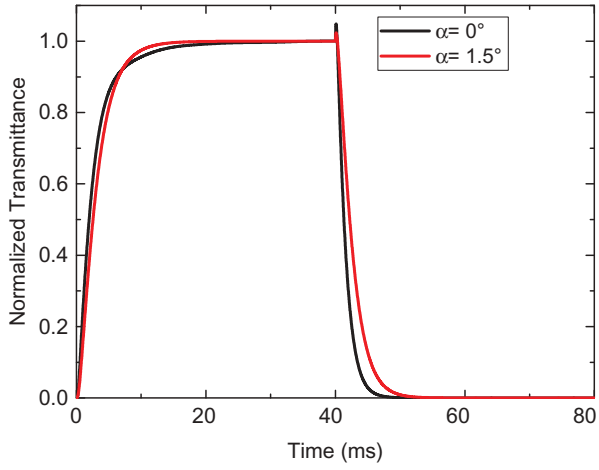

Figure 6. Simulated response time curves of d-FFS at α = 0° and 1.5°.

4.2. Electrode structure optimisation

To find the optimal device parameters, we perform simulation with different electrode width and electrode gap for the d-FFS LCD with α = 1.5°. Figure 7(a) shows the simulated VT curves where electrode width (w) varies from 2.0 to 4.0 μm, while keeping electrode gap (g) at 3.0 μm.

As Figure 7(a) depicts, the peak transmittance decreases gradually as the electrode width increases from 2.0 to 4.0 μm due to the enlarged dead zone area. However, the on-state voltage only slightly shifts from 5.4 to 5.6 V, as it is less sensitive when a small Δε LC is employed [26]. Figure 7(b) shows the simulated VT curves where electrode gap varies from 2.0 to 4.0 μm while keeping electrode width at 2.0 μm. As the electrode gap increases, transmittance decreases because more LC directors at the centre of electrode do not reorient. We also find that the response time does not vary much as the electrode width and electrode gap change from 2.0 to 4.0 μm. For the d-FFS with w = 2.0 μm and g = 2.0 μm, the simulated peak transmittance is 85.2%, rise time ≈5.62 ms and decay time ≈4.77 ms at V_{on} = 5.8V_{rms}.

Table 2 compares the performance of our proposed device with two prior LC devices: Device I and Device II. The goal of this analysis is to distinguish the improvement from material and device structure. For Device I, a positive Δε LC material and interdigitated pixel electrode structure with alternative tilt are used [23]. Device II has the same

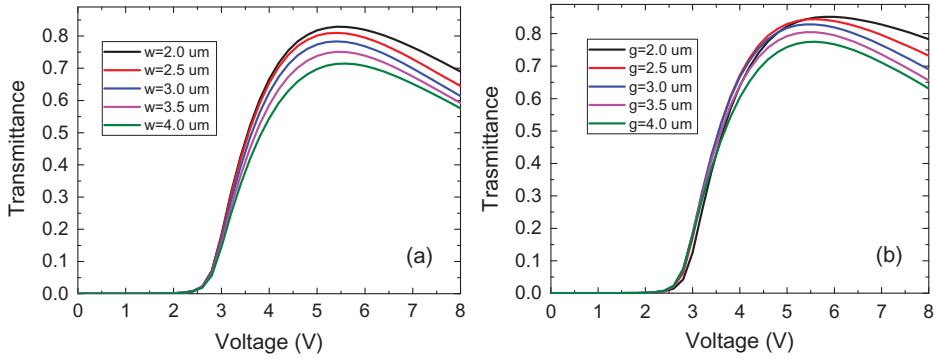

Figure 7. Simulated VT curves of d-FFS using M1. (a) Keeping electrode gap at 3.0 μm while varying electrode width from 2.0 to 4.0 μm. (b) Keeping electrode width at 2.0 μm while varying electrode gap from 2.0 to 4.0 μm.

Table 2. Calculated peak transmittance and response time at the on voltage for three LC devices.

LC Device	Rubbing angle	Voltage (V)	Transmittance	Rise (ms)	Decay (ms)
Device I	0°	5.0	47.0%	5.9	3.2
	1.5°	5.2	69.5%	7.0	6.1
Device II	0°	6.6	47.0%	5.2	2.5
	1.5°	6.4	79.4%	6.7	4.7
Proposed device	0°	6.2	51.1%	5.0	2.4
	1.5°	5.8	85.2%	5.6	4.8

configuration as Device I, except that the employed LC material is replaced by our M1 mixture. For a fair comparison, we use the same electrode width (2.0 μm), electrode gap (2.0 μm) and cell gap (2.5 μm). While comparing Device II with Device I, we find that the rise time and decay time are all reduced for both α = 0°and α = 1.5°. This is because M1 has a lower viscosity (35.75 mPas vs. 47.6 mPas). Moreover, for the case of α = 1.5°, the transmittance of Device II is higher than that of Device I (79.41% vs. 69.52%). The enhanced transmittance is the product of smaller Δε [27] and higher $\varepsilon_{\perp}/\varepsilon_{//}$ratio [28] of our M1 mixture. However, a major trade-off is increased on-state voltage because M1 has a smaller Δε (2.66 vs. 5.1) in Device II. When comparing our proposed device with Device II (using the same M1 mixture), we find the improvement is in three areas: (1) the transmittance is improved from 79.4% to 85.2%, (2) the on-state voltage is decreased from 6.4 to 5.8 V and (3) the response time (rise + decay) is slightly faster (from 11.4 to 10.4 ms). The lower operation voltage is due to the electrode shape and uniform tilt and twist angles of LC directors in the voltage-on state.

5. Discussion

In order to get high transmittance, fast response time and low operation voltage, we have introduced an improved mixture to our d-FFS mode. Our LC material exhibits a low viscosity which helps to reduce response time. However, the trade-off is its low Δε, which leads to increased operation voltage. With our diamond-shaped electrodes, we are able to keep a high transmittance (~85%) at 5.8 V. To lower the operating voltage to 5 V (similar to that of most commercial LCDs), we need to increase Δε by ~35%, which would slightly increase the viscosity. It is worth mentioning that the electric field in our d-FFS mode is at an oblique angle to the LC directors, which eliminates the requirement of non-zero pretilt angle for forming two-domain LC confinement. Figure 8(a,b) shows the cross-sectional view of LC director configuration and the corresponding transmittance at a voltage-on state for α = 0° and α = 1.5°, respectively. In Figure 8(a), because the rubbing angle is zero, the virtual walls above the electrodes provide additional restoring force to the LC directors. Hence, fast response is obtained. However, dead zones are formed at the same time, leading to a relatively low transmittance. To boost transmittance, we investigated the device configuration with α = 1.5°. As Figure 8(b) depicts, the LC directors above the electrodes are also reoriented by the electric field, which reduces the dead zone area. In addition, the spatial shift between adjacent pixels and common electrodes helps to spread the electric field more uniformly, which also contributes to the increased transmittance. Our d-FFS with α = 1.5° rubbing angle is very preferable in terms of transmittance while the trade-off in response time is minimal. In the following sections, we will show the calculated GTG response time, MPRT, viewing angle, gamma shift and colour shift for our d-FFS at α = 0° and α = 1.5° rubbing angle with optimised structure.

5.1. Grey-to-grey (GTG) response time

We divide the VT curve uniformly into 256 grey levels based on gamma-2.2 rule in order to obtain the response time between different grey levels. We study the transitions between 0, 64, 128, 192 and 255 grey levels. The GTG response time (rise and decay) is defined between 10% and 90% transmittance change. The simulated GTG response times are listed in Tables 3 and 4 for α = 0° and

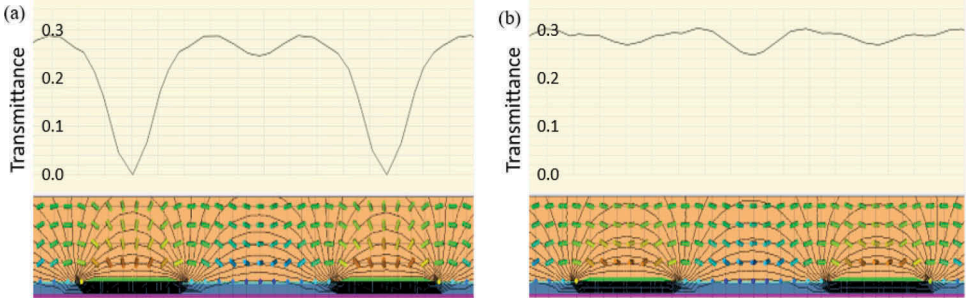

Figure 8. Cross-sectional view of the simulated LC director distributions and local relative transmittance of d-FFS cell at (a) α = 0° and (b) α = 1.5° rubbing angle.

Table 3. Calculated GTG response time of our proposed d-FFS with α = 0°.

Voltage	0 V	3.08 V	3.46 V	4.04 V	6.20 V
Grey level	**0**	**64**	**128**	**192**	**255**
0		13.19	8.5	5.42	4.95
64	1.93		7.66	5.12	4.37
128	1.97	8.12		4.69	4.49
192	2.08	6.12	5.31		4.67
255	2.43	5.85	5.68	4.44	

Table 4. Calculated GTG response time of our proposed d-FFS with α = 1.5°.

Voltage	0 V	2.75 V	3.10 V	3.55 V	5.80 V
Grey level	**0**	**64**	**128**	**192**	**255**
0		16.15	14.70	11.56	5.62
64	3.85		10.69	10.52	5.31
128	4.02	11.19		9.49	5.09
192	4.19	12	10.67		5.31
255	4.77	11.76	10.45	8.98	

α = 1.5°, respectively. From Tables 3 and 4, the average GTG response time is found to be 5.35 ms for α = 0°, and 8.81 ms for α = 1.5°. The faster average GTG response time for α = 0° is expected because of the virtual walls. However, its transmittance is greatly sacrificed.

To evaluate image blurs of a TFT-LCD or OLED, MPRT should be considered. For a TFT-LCD, its MPRT depends on the LC response time and TFT frame rate as [7]:

$$MPRT \approx \sqrt{\tau^2 + (0.8 \times T_f)^2}. \quad (4)$$

In Equation (4), τ is the LC response time and T_f (= 1000/f) is the TFT frame time. Based on Equation (4), if the FFS device is driven at 144 Hz, then its corresponding average GTG MPRT should be 7.82 and 10.41 ms at α = 0° and α = 1.5°, respectively. Both are too slow and image blur would be inevitable. To suppress image blurs to unnoticeable level, we set CRT-like MPRT as the criterion, which is 1.5 ms. From Equation (4), if $\tau \approx 5$ ms, then it is impossible to reduce the MPRT to 1.5 ms, even we increase the frame rate. Another drawback for increasing frame rate is the dramatically shortened TFT charging time, especially for a high-resolution (4K2K) display. A more effective way to reduce MPRT is to decrease the duty ratio [29,30]. Especially, when the duty ratio is low, MPRT is less sensitive to the LC response time. This is because the backlight is turned on at a later stage so that the beginning slow response is more forgiven. However, decreasing the duty ratio would lower the display luminance proportionally. Table 5 shows the required duty ratio and resultant display transmittance in order to obtain MPRT = 1.5 ms at 90-Hz and 120-Hz frame rates for α = 0° and α = 1.5°. From Table 5, at 90 Hz we need to reduce the duty ratio to 17% for both α = 0° and α = 1.5° in order to obtain MPRT = 1.5 ms. Under such a circumstance, the corresponding effective transmittance is 0.086 for α = 0° and 0.144 for α = 1.5°. That means, the device with α = 1.5° exhibits a 67% higher transmittance than that with α = 0°. Similar improvement (67%) in transmittance is also found at 120-Hz framerate. This is why the high transmittance of our proposed FFS device with α = 1.5° is so much more favourable than that with α = 0°, although the latter has a faster response time.

5.2. Viewing angle

As Figure 3(b) shows, the gaps (white areas) between electrodes exhibit zig-zag structure. That means, each pixel actually exists multi-domain structure, which helps to widen the viewing angle. We use a positive A-plate and a positive C-plate as compensation films. Their refractive indices and film thickness are listed as follows: $n_{e,+A}$ = 1.5110, $n_{o,+A}$ = 1.5095, $n_{e,+C}$ = 1.5110, $n_{o,+C}$ = 1.5095, d_{+A} = 92.59 μm, and d_{+C} = 60.09 μm. Figure 9(a,b) depicts the simulated isocontrast contour of our d-FFS LCD with compensation films at α = 0° and α = 1.5°, respectively. For α = 1.5°, maximum contrast ratio over 5000:1 is obtained and it expands to a larger zone when compared to α = 0° where maximum contrast ratio is 3357:1. In both cases, the contrast ratio over 500:1 expands to ~70° viewing cone and it remains over 100:1 in the entire viewing cone.

5.3. Gamma curve

In addition to high transmittance, fast MPRT and wide viewing angle, small gamma shift is also critically important for a display device. To quantify gamma shift, an off-axis image distortion index (D) has been defined [31]. Figure 10(a,b) shows the simulated gamma curves of our d-FFS LCD at four specified viewing angles for α = 0° and α = 1.5°, respectively. Along the 0° azimuthal angle, we

Table 5. Calculated duty ratio and display effective transmittance for achieving 1.5-ms MPRT.

Rubbing angle	LCD Trans. (%)	MPRT (ms)	Backlight on-time (ms)	LC response time (ms)	Frame rate (Hz)	Frame time (ms)	Duty ratio	Effective Trans. (%)
0°	51.1	1.50	1.88	5.35	90	11.1	0.17	8.6
	51.1	1.50	1.88	5.35	120	8.3	0.23	11.5
1.5°	85.2	1.50	1.88	8.81	90	11.1	0.17	14.4
	85.2	1.50	1.88	8.81	120	8.3	0.23	19.2

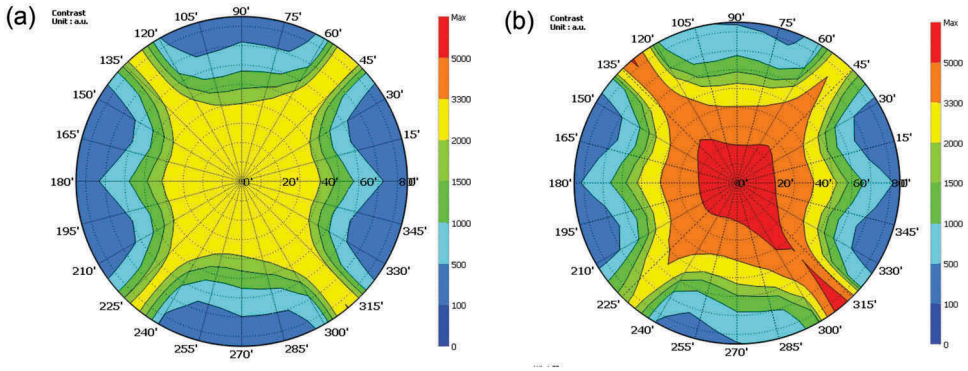

Figure 9. Simulated isocontrast contour of d-FFS LCD with (a) α = 0° and (b) α = 1.5° using a positive A-plate and a positive C-plate.

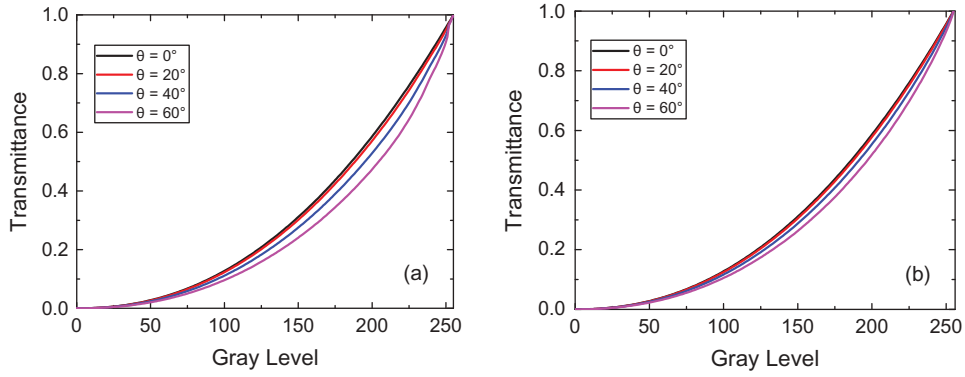

Figure 10. Simulated gamma shift of the film-compensated d-FFS LCD at (a) α = 0° and (b) α = 1.5°.

find D(60°, 0°) = 0.182 for α = 0° and D = 0.113 for α = 1.5°. In both scenarios, D is smaller than 0.2, which means the gamma shift of our d-FFS LCD is indistinguishable by the human eye [32].

5.4. Colour shift

Indistinguishable colour shift is another critical requirement of all display devices. By using a quantum dot enhancement film [33,34], we calculated the colour shift of our d-FFS LCD at different viewing angles. Colour shift in Δu′v′ colour coordinate system at different polar angles (at 0° azimuthal angle) are shown in Figure 11(a,b) at α = 0° and α = 1.5°, respectively. From Figure 11, the colour difference for RGB wavelengths is smaller than 0.008 even at ~ 80° viewing cone. When Δu′v′ is smaller than 0.02, it is indistinguishable to the human eye.

6. Conclusion

We have reported a positive Δε LC mixture and a diamond-shaped pixel configuration for FFS mode.

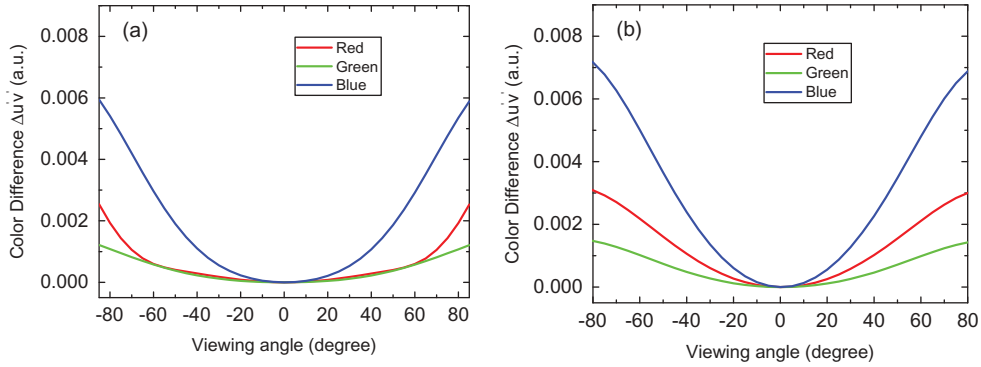

Figure 11. Simulated colour shift at (a) α = 0° and (b) α = 1.5° using a quantum dot-enhanced backlight.

High transmittance (T_{max} ~85%), fast response time (average GTG ~2.92 ms) and low operation voltage (5.8V) have been achieved. High transmittance and fast LC response time are critical for high-resolution density and high frame rate displays to keep low power consumption and to mitigate image blurs. We have also achieved high contrast ratio, wide view and indistinguishable colour shift and gamma shift by using compensation films. Considering these outstanding features, our proposed d-FFS LCD should have potential for many practical applications.

Acknowledgments

The authors would like to thank Haiwei Chen, Guanjun Tan and Fangwang Gou for helpful discussion.

Disclosure statement

No potential conflict of interest was reported by the authors.

Funding

This work was funded by Air Force Office of Scientific Research (AFOSR) (FA9550-14-1-0279).

References

[1] Schadt M. Milestone in the history of field-effect liquid crystal displays and materials. Jpn J Appl Phys. 2009;48:03B001.
[2] Tsujimura T. OLED display fundamentals and applications. 2nd ed. Chichester (UK): Wiley; 2017.
[3] Hua H. Enabling focus cues in head-mounted displays. Proc IEEE. 2017;105(5):805–824.
[4] Chen H, Gou F, Wu ST. A submillisecond-response nematic liquid crystal for augmented reality displays. Opt Mater Express. 2017;7(1):195–201.
[5] Chen H, Lee JH, Lin BY, et al. Liquid crystal display and organic light-emitting diode display: present status and future perspectives. Light Sci Appl. 2018;7:17168.
[6] Igarashi Y, Yamamoto T, Tanaka Y, et al. Summary of moving picture response time (MPRT) and futures. SID Int Symp Digest Tech Papers. 2004;35(1):1262–1265.
[7] Peng F, Chen H, Gou F, et al. Analytical equation for the motion picture response time of display devices. J Appl Phys. 2017;121(2):023108.
[8] Murawski C, Leo K, Gather MC. Efficiency roll-off in organic light-emitting diodes. Adv Mater. 2013;25:6801–6827.
[9] Féry C, Racine B, Vaufrey D, et al. Physical mechanism responsible for the stretched exponential decay behavior of aging organic light-emitting diodes. Appl Phys Lett. 2005;87:213502.
[10] Lee SH, Lee SL, Kim HY. Electro-optic characteristics and switching principle of a nematic liquid crystal cell controlled by fringe field switching. Appl Phys Lett. 1998;73(20):2881–2883.
[11] Deng Z, Zheng B, Zheng J, et al. High dynamic range incell LCD with excellent performance. SID Symp Dig Tech Papers. 2018;49(1):996–998.
[12] Tan G, Huang Y, Chen MC, et al. High dynamic range liquid crystal displays with a mini-LED backlight. Opt Express. 2018;26(13):16572–16584.
[13] Jiao M, Ge Z, Wu ST, et al. Submillisecond response nematic liquid crystal modulators using dual fringe field switching in a vertically aligned cell. Appl Phys Lett. 2008;92:111101.
[14] Matsushima T, Seki K, Kimura S, et al. New fast response in-plane switching liquid crystal mode. J Soc Inf Disp. 2018;26(10):602–609.
[15] Choi TH, Oh SW, Park YJ, et al. Fast fringe-field switching of a liquid crystal cell by two-dimensional confinement with virtual walls. Sci Rep. 2016;6:27936.
[16] Katayama T, Higashida S, Kanashima A, et al. Development of in-plane super-fast response (ip-SFR) LCD for VR-HMD. SID Int Symp Digest Tech Papers. 2018;49(1):671–673.
[17] Takatsu H Advanced liquid crystal materials for active matrix displays. Proceedings of the Advanced Display Materials and Devices; 2014 Jul 23–25; Sendai, Japan.
[18] Haller I. Thermodynamic and static properties of liquid crystals. Prog Solid State Chem. 1975;10(2):103–118.
[19] Wu ST. Birefringence dispersions of liquid crystals. Phys Rev A. 1986;33(2):1270–1274.
[20] Wu ST, Wu CS. Rotational viscosity of nematic liquid crystals a critical examination of existing models. Liq Cryst. 1990;8(2):171–182.
[21] Xu D, Peng F, Tan G, et al. A semi-empirical equation for the response time of in-plane switching liquid crystal and measurement of twist elastic constant. J Appl Phys. 2015;117:203103.
[22] Chen H, Lan YF, Tsai CY, et al. Low-voltage blue-phase liquid crystal display with diamond-shape electrodes. Liq Cryst. 2017;44(7):1124–1130.
[23] Choi TH, Woo JH, Choi Y, et al. Interdigitated pixel electrodes with alternating tilts for fast fringe-field switching of liquid crystals. Opt Express. 2016;24(24):27569–27576.
[24] Lien A. Extended Jones matrix representation for the twisted nematic liquid crystal display at oblique incidence. Appl Phys Lett. 1990;57(26):2767–2769.
[25] Ge Z, Wu ST, Kim SS, et al. Thin cell fringing-field-switching liquid crystal display with a chiral dopant. Appl Phys Lett. 2008;92:181109.
[26] Chen H, Peng F, Luo Z, et al. High performance liquid crystal displays with a low dielectric constant material. Opt Mater Express. 2014;4(11):2262–2273.
[27] Ryu JW, Lee JY, Kim HY, et al. Effect of magnitude of dielectric anisotropy of a liquid crystal on light efficiency in the fringe-field switching nematic liquid crystal cell. Liq Cryst. 2008;35(4):407–411.
[28] Kang SW, Jang IW, Kim DH, et al. Enhancing transmittance of fringe-field switching liquid crystal device by controlling perpendicular component of dielectric constant of liquid crystal. Jpn J Appl Phys. 2014;53(1):010304.

[29] Ito H, Ogawa M, Sunaga S. Evaluation of an organic light-emitting diode display for precise visual stimulation. J Vis. 2013;13(7):6.
[30] Gou F, Chen H, Li M, et al. Motion-blur-free LCD for high resolution virtual reality displays. J Soc Inf Disp. 2018;26 (4):223–228.
[31] Park SB, Song JK, Um Y, et al. Pixel-division technology for high-quality vertical-alignment LCDs. IEEE Electron Device Lett. 2010;31(9):987–989.
[32] Kim SS, Berkeley BH, Kim KH, et al. New technologies for advanced LCD-TV performance. J Soc Inf Disp. 2004;12 (4):353–359.
[33] Luo Z, Xu D, Wu ST. Emerging quantum-dots-enhanced LCDs. J Disp Technol. 2014;10(7):526–539.
[34] Chen H, He J, Wu ST. Recent advances in quantum-dot-enhanced liquid crystal displays. IEEE J Sel Topics Quantum Electron. 2017;23(5):1900611.